Thermochemical conversion of biomass volatiles via chemical looping: Comparison of ilmenite and steel converter waste materials as oxygen

(article starts on next page)

Thermochemical conversion of biomass volatiles via chemical looping: Comparison of ilmenite and steel converter waste materials as oxygen carriers

Ali Hedayati [a], Amir H. Soleimanisalim [b], Tobias Mattisson [b], Anders Lyngfelt [b,*]

[a] TECNALIA, Basque Research and Technology Alliance (BRTA), Alava Science and Technology Park, Leonardo da Vinci 11, 01510 Vitoria-Gasteiz, Spain
[b] Chalmers University of Technology, Division of Energy Technology, Hörsalsvägen, 7B, 412 58 Göteborg, Sweden
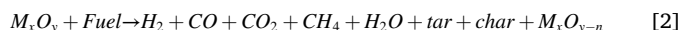
ARTICLE INFO

ABSTRACT

Two oxygen carriers were tested with respect to chemical looping combustion (CLC) and chemical looping gasification (CLG). Ilmenite, a natural ore composed mainly of iron–titanium oxide, and LD Slag, an iron-based industrial waste, were investigated at 850 and 900 °C in a continuous operation in a 0.3 kW chemical-looping reactor system using synthetic biomass volatiles as fuel. CLC and CLG conditions were simulated in the fuel reactor by changing the fuel flow rates. In the case of ilmenite the syngas yield and methane conversion increased with fuel flow rate. Consequently, the syngas to hydrocarbon ratio was higher for ilmenite. Methane conversion improved for both tested oxygen carriers with increasing the operating temperature. Oxygen release was observed in the case of LD Slag. The H_2/CO ratio was between 0.7 and 0.8 for both oxygen carriers at the higher fuel flows. With respect to CLC, ilmenite showed higher gas conversion than LD slag. Analysis of the particles revealed that ilmenite possessed better mechanical properties and formed less dust compared to LD Slag during the continuous operation with fuel.

1. Introduction

CO$_2$ capture and storage (CCS) have been recognized internationally as one of the essential options for climate mitigation [1,2]. CCS technologies have had a focus on fossil fuels, but it is even more critical to use CCS with bioenergy, so called bio-energy carbon capture and storage (BECCS), in order to remove CO$_2$ from the atmosphere [3,4]. BECCS will result in net negative emission which is necessary to meet recently decided climate targets such as the Paris Agreement (2015). Among CO$_2$ capture technologies proposed for BECCS, Chemical-looping combustion (CLC) of solid fuels is a potential break-through CO$_2$ capture technology which is unique in avoiding significant costs and energy penalties associated with gas separation [5–8]. The CLC system is composed of two interconnected fluidized bed reactors, i.e. an air reactor (AR) and a fuel reactor (FR) where oxygen carriers in the form of metal oxide particles transfer oxygen between the two reactors (see Fig. 1) [7]. In the fuel reactor, a fuel reacts with the oxygen carrier (bed materials in the form of a metal oxide Me$_x$O$_y$) and in the air reactor, the oxygen carrier is oxidized (see equation 1) with air. The products of the

FR are ideally H$_2$O and CO$_2$ whereupon condensation of water a stream of CO$_2$ can be obtained. Therefore, the capture of CO$_2$ is inherent in the CLC process. Chemical-Looping Gasification (CLG) is a gasification technology based on the CLC process where partial oxidation of the fuel is achieved by reducing oxygen availability in FR to produce a syngas of mainly CO and H$_2$ [9,10]. Chemical looping reforming (CLR), where the purpose is to convert a hydrocarbon containing gaseous fuel, to syngas, is another example of chemical looping [11]. Syngas can be further used as a source of hydrogen or as a feedstock for the production of other liquid biofuels [12]. In CLG, the biomass is pyrolyzed and gasified in the fuel reactor, and the oxygen carrier (M$_y$O$_x$) can react with the intermediate gaseous species such as CH$_4$ and C$_2$H$_{2n}$ to form syngas, CO$_2$ and H$_2$O [13] (see Eq. 2).

$$M_xO_{y-n} + \frac{n}{2}O_2 \rightarrow M_xO_y \qquad [1]$$

$$M_xO_y + Fuel \rightarrow H_2 + CO + CO_2 + CH_4 + H_2O + tar + char + M_xO_{y-n} \qquad [2]$$

CLG is similar to normal indirect gasification, and at optimal conditions, there will be no combustion of fuel in the air reactor; therefore, a

---

Nomenclature

BECCS	bio-energy carbon capture and storage		spectrometry
BMV	biomass volatiles	λ_{eff}	effective air ratio
f_i	carbon fraction of i (CO, CO_2, CH_4, C_2 or C_3), Eq. 8 (-)	LHV	lower heating value
CCS	carbon capture and storage	φ_i	FR conversion ratio (-)
f_{syngas}	Syngas fraction, Eq. 7 (-)	M_xO_y	oxidized metal oxide
CLC	chemical looping combustion	$\varnothing_0$	Molar ratio (-)
T	temperature (°C)	M_xO_{y-1}	reduced metal oxide
CLG	chemical looping gasification	Ω_{OD}	oxygen demand (-)
x_i	concentration of species i (mol/mol)	PSD	particle size distribution
EB	Elwaleed-B	OFR	oir to fuel ratio
y_i	carbon content of species i (-)	SC	Sibelco Calcined
FR	fuel reactor	AR	air reactor
η_{gas}	gas conversion efficiency	SEM	scanning electron microscope
ICP + SFMS	inductively coupled plasma-sector field mass	XRD	X-ray (powder) diffraction

high degree of carbon capture can be achieved. The use of oxygen carriers in CLG has several advantages over conventional dual fluidized bed gasification processes: i) in CLG, metal oxides provide catalytic sites for reforming reactions, ii) higher concentration of CO_2 and H_2O suppresses tar formation, iii) metal oxides may provide additional sites to enhance hydrocarbon conversion to syngas, and iv) in case of applying contaminated alternative solid fuels such as wastes, the FR can act as a sink for trapping and conversion of aggressive and toxic impurities [5,13–16]. The former is particularly important in the case of alkali and chlorine compounds in biomass-fired systems [17]. In addition, as no combustion will take place in the air reactor, corrosion here can be limited, which could be highly advantageous [13]. To achieve autothermal CLG operation condition, a significant fraction of the carbon will need to be converted to CO_2 in the FR. This is another advantage of CLG compared to indirect gasification, where a large fraction of this CO_2 is generated in the air or combustion reactor, thus being diluted with nitrogen. The principles of CLC and CLG are illustrated in Fig. 1.

The technology readiness level (TRL) of CLC of solid fules is currently at TRL 6 with successful continuous operation up to 1 MW$_{th}$ and for CLG of solid fuels is at TRL 5 with operation up to 10 kW$_{th}$ [18,19]. Most operational experience with chemical looping has been carried out with a focus on fossil-based fuels [6,20,21]. Researches on the use of biomass as a solid fuel in CLC and CLG have been increasing recently with respect to the aspects of negative CO_2 emission [13]. Moldenhauer et al. tested steam-exploded pellets and wood char in a 10 kW CLC unit where a CO_2 yield of 92% was reported at 965 °C [5]. Gogolev et al. tested four biomass fuels of varied alkali content in the 100 kW CLC unit at Chalmers University of Technology using a mixture of natural and synthetic oxygen carriers [22]. They focused on the fate of alkali and concluded that most of the alkali content of the biomass was accumulated in the oxygen carriers. Samprón et al. [9] tested Fe-based oxygen

carriers using pine wood as fuel in a 1.5 kW continuous CLG unit and reported around 60% syngas yield with H_2/CO ratio of approximately two at autothermal conditions. Very low tar content was found during the CLG operation, but the formation of fines was reported as a drawback of CLG compared to CLC. Ilmenite as an oxygen carrier was tested by Condori et al. [23] for CLG of pine wood in the same unit used by Samprón et al. [9], which compared ilmenite as a natural ore and synthetic iron-based oxygen carriers. Ilmenite showed less reactivity toward the conversion of CH_4, C_2 and C_3 species and the syngas yield, in the case of ilmenite, was 50% at the highest [23]. Condori et al. [23] had 55 h of continuous CLG operation in 1.5 kw$_{th}$ unit using ilmenite as an oxygen carrier. They proved that CLG can produce high quality syngas with and authothermal condition and a tar content below 2 gNm^{-3} which is a relevant advantageous of CLG.

Fundamental for the chemical-looping technologies is the use of suitable oxygen carriers that fulfil several requirements, i.e. high reactivity in both reduction and oxidation, sufficient mechanical strength, low agglomeration tendency, long lifetime, and low cost [24]. In addition, these materials should be environmentally benign [25,26]. Numerous oxygen carriers based on Cu, Co, Mn, Fe, and Ni have been studied for the chemical looping of gaseous fuels during the last 20 years [27,28]. In this regard, natural ores of manganese and iron are at the center of attention for chemical-looping technology owing to their low cost and proven reactivity [3,5]. In our previous work, we investigated two manganese ores for chemical looping conversion of synthetic biomass volatiles in a 300 W reactor system. Both manganese ores showed high conversion of biomass volatile gases and high temperature and fuel rate favored syngas yield in the outlet stream of the FR [29]. Industrial iron-based by-products and wastes have recently attracted attention as oxygen carriers for chemical looping applications due to benefits such as low cost and possibility of reuse and utilization of
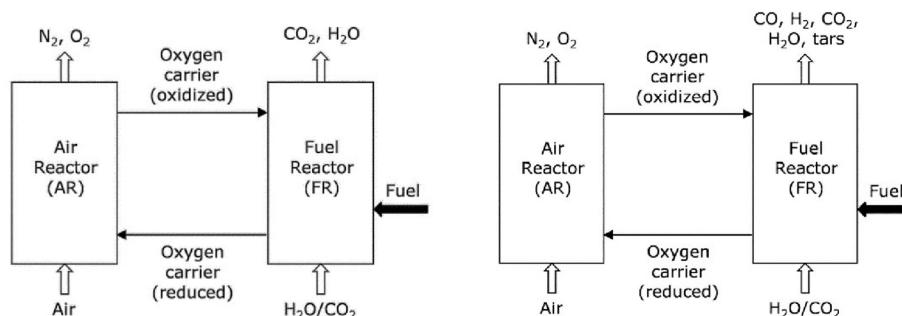

Fig. 1. Chemical-looping combustion (left) and chemical-looping gasification (right) principles [5].

industrial waste for clean energy generation and carbon capture. To date, there are only a few reports on the use of waste iron-based by-products from the steel industry as oxygen carriers in CLC and CLG [5,13,30]. In CLG, these materials are required to sustain high conversion rates toward CH_4, C_2 and C_3 species to H_2 and CO. In CLG, oxygen carrier particles might leave the AR in a not fully oxidized state at CLG conditions and undergo a further reduction in the FR. Therefore, sufficient mechanical stability and durability are needed to avoid particle crashing and fines formation during CLG. Concerning CLR, the majority of the reported literature is based on methane reforming for hydrogen and syngas production focusing on Fe, Cu, and Ni based oxygen carriers in fixed bed reactor systems [21,31].

1.1. LD Slag as oxygen carrier for chemical looping

LD Slag is a ground steel converter slag from the Linz–Donawitz process. Millions of tons of LD Slag are produced yearly, of which a large amount is disregarded and landfilled as waste with no further use [32]. The major components in LD Slag are oxides of Ca (30–60%), Fe (10–35%), and Si (8–20%) with some amounts of Mg, Mn, Al, V, and Ti depending on the origin of the iron ore [33]. The low price and relatively high iron contact of LD Slag could make it relevant for application in chemical looping processes. Besides, co-existence of Ca-Fe-O phases has been reported to increase the fraction of syngas in CLG [34]. Moldenhauer et al. [5] tested LD Slag for CLC of syngas, methane and CLG of biomass fuels. Full conversion of syngas at 900 °C and 60% methane conversion at 950 °C were obtained. Mattisson et al. [13] investigated the conversion of CO, H_2, CH_4, and C_2H_4 with LD Slag at 800–950 °C using synthetic biogas in a batch fluidized bed reactor. Recently, Condori et al, [35] used LD slag as an oxygen carrier for CLG in 1.5 kW_{th}. They reported biomass conversion above 90% with high quality syngas and no agglomeration during 60 h of CLG operation. LD Slag was also used as bed material in the 12 MW Circulating Fluidized Bed (CFB) biomass boiler at Chalmers University of Technology to order to investigate Oxygen Carrier Aided Combustion (OCAC) [33]. The general conclusions are i) LD Slag is reactive in CO conversion; ii) LD Slag has shown limited reactivity toward hydrocarbon conversion; and iii) thanks to the presence of Ca in LD slag, it can promote the water–gas-shift reaction toward more hydrogen production [33]. Therefore, LD slag can be a good candidate to be sued for CLG and CLC; however, its behavior towards biomass volatile matter conversion has not been thoroughly investigated.

1.1.1. Scope and aim

As discussed in the previous section, the behavior of LD Slag in the chemical looping process is promising, given that it is an industrial iron and calcium-based waste material. However, a further study of LD Slag as an oxygen carrier in a more controlled way is necessary to evaluate all the aspects of its performance in CLC and CLG processes. The aim of this work is to investigate the performance of LD Slag as an oxygen carrier in the conversion of biomass volatiles and their suitability for large scale operation. This is done by performing experiments in a dual fluidized bed reactor and at different reduction degrees of oxygen carriers by setting the flow rates of the fuel. For the sake of comparison with a benchmark material, ilmenite is also investigated in parallel with LD Slag and as a reference oxygen carrier. Ilmenite was selected since it is also an iron-based material that has been extensively studied due to low cost, good fluidizability, high melting point, and low production of fines [27]. In this work, the reactivity of the LD slag and ilmenite in terms of gas conversion, syngas fraction, CO_2 yield, attrition characteristics, and phase changes is studied. In this regard, a special gas blend is used which represents the resulting volatile matter, i.e. the gas released from biomass when it is introduced to the fuel reactor.

2. Materials and methods

2.1. Oxygen carrier materials

LD Slag (a waste product from the steel industry) and Norwegian Ilmenite (an iron–titanium ore, referred to as *Ilm* in the tables and figures) were used in this study. LD Slag was delivered by SSAB Merox, Sweden. The elemental composition of LD Slag and Ilmenite is given in Table 1. Oxygen carriers were calcined in air at 950 °C for 24 h to ensure full oxidation. The calcined particles were sieved to obtain around 0.5 kg of particles smaller than 212 μm, to be loaded into the 300 W reactor. Particles calcined in the air are denoted *Fresh* and particles recovered from the reactor after the experiments are denoted *Used*. The latter were oxidized by operating the reactor system with air after stopping the fuel addition.

2.2. Characterization of oxygen carriers

Elemental composition and oxide phases of the oxygen carriers were analyzed using ICP-SFMS (Inductively Coupled Plasma – Sector Field Mass Spectrometry) and X-Ray power diffraction (Siemens 5000 X-Ray diffractometer), respectively. Bulk density of the fresh and used particles was measured according to ISO standard 3923-1 by pouring the metal oxide of <212 μm into a cylinder of defined volume through a funnel and weighing the mass of particles in the cylinder. As an indicator of the attrition and agglomeration of the particles during the operation, the particle size distribution of the fresh and used particles was obtained by sieving the particles in the range of 45, 90, 125, 150, 180, and 212 μm. Particles smaller than 45 μm are considered as fines in this work. The outlet streams of the AR and FR were filtered to trap and collect the fines that were formed during the operations. Given the total hours of operation, the attrition rate of the oxygen carriers was calculated as the rate of the mass loss of fines per hour divided by the initial mass of the particles loaded into the reactor.

2.3. 300 W chemical looping fluidized bed reactor

Experiments were done in a 300 W CLC reactor where the oxygen carriers are investigated with gaseous fuel under the continuous circulation of particles together with fuel. The schematic illustration of the 300 W chemical-looping reactor used in this work is shown in Fig. 2.

The reactor system is made of 253MA high temperature chromium-nickel stainless steel alloy suitable for severe conditions. Previous experience with this material in CLC pilots indicates that the material has a lifetime at least well exceeding 1000 h of operation. The reactor is 300 mm high with a cross-section of 25 mm × 25 mm for the fuel reactor (FR) and 25 mm × 42 mm for the air reactor (AR). The AR has a narrower riser of 25 mm × 25 mm and is operated at a gas velocity sufficient to transport the particles upwards, thus accomplishing the circulation of bed material. There is a gap between the two reactors to minimize the risk of leakage between them. There are two wind boxes located in the bottom of each reactor to let the gas into each reactor via porous quartz plates which act as gas distributors. There is a top part over each reactor where the cross-section of both reactors increases to let the gas velocity decrease so that particles fall back into the reactors. On the AR side, part of the particles drops into a loop seal that connects the AR to FR. On the FR side, particles drop directly back into the FR. The loop seals are fluidized with inert gas. From the bottom of the FR, particles pass through the lower loop-seal and return to the AR where the cycle starts

Table 1
Elemental composition of fresh oxygen carriers excluding oxygen (wt%).

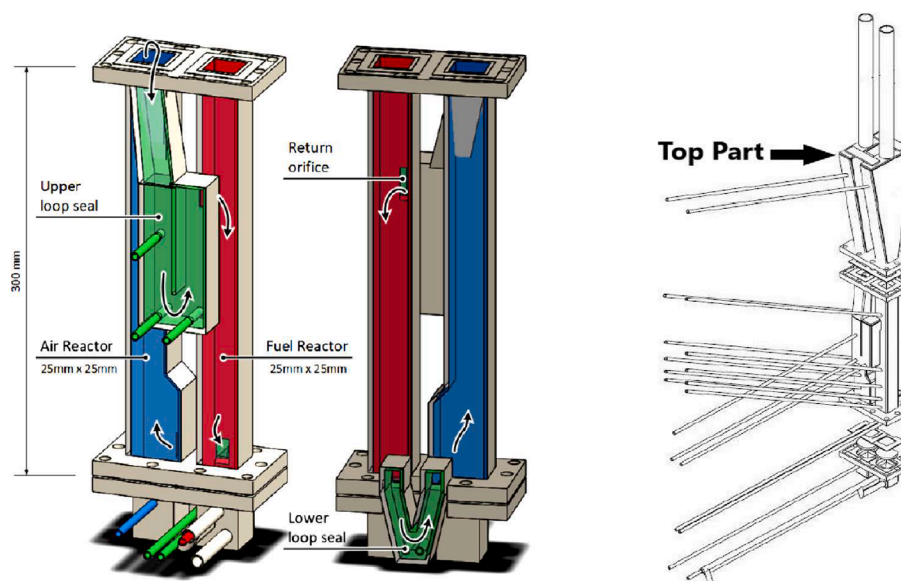|	Ca	Fe	Mg	Si	Mn	V	Ti
LD Slag	27.3	13.7	6.0	4.8	2.2	1.6	0.7
Ilmenite	0.2	34.5	2.2	0.9	0.2	–	26.9

Fig. 2. 300 W reactor (left) and its technical drawing (right) [36].

over, and the loop is complete. The loop seals are purged with 650 mL·min^{-1} (higher + lower loop seals) of air or argon (when operating with fuel) to ensure the fluidization and circulation of the particles. The exit pipe of the FR is connected to a water seal with a column height of<2 cm to keep a higher pressure of 0.1–0.2 kPa, in the FR compared to AR in order to reduce gas leakage from AR to FR. The bed temperatures of AR and FR are measured by means of K-type thermocouples. The 300 W reactor is located inside an electrical furnace that controls the temperature. The fluidization and particle circulation are monitored via pressure difference measurement at different heights of AR and FR.

2.4. Experimental procedure

Prior to the experiments, oxygen carriers were activated with syngas, 50% hydrogen in CO, at 900 °C for 2–3 h. Oxygen carriers were circulating during the activation and the AR air flow rate was 8 L·min^{-1}. The indicator of the activation is the stable concentration of CO_2 out from the FR. Biomass volatiles (BMV) which are released upon heating, typically constitute 80 wt% of the original fuel on a dry basis [3]. In this work a synthesized gas mixture was used to simulate biomass volatiles (BMV) for the experiments in the 300 W reactor. This composition was chosen to represent the gases generated via the devolatilization of wood-based biofuels. This composition resembles the gas generated during the operation of the Chalmers 2 MW gasifier, albeit excluding tars and higher hydrocarbons [37]. The composition of BMV fuel is given in Table 2.

Four BMV flow rates were selected to investigate gas conversion, the H_2/CO ratio, and the attrition and mechanical behavior of the particles. The selected BMV flow rates are 0.6, 0.9, and 1.2, and 2 L·min^{-1} corresponding to an overall oxygen-to-fuel-ratio (OFR) of 3.2 – 0.9 given that the air flow rates in the AR was set at 9 L·min^{-1}. The OFR is the ratio between number of moles of oxygen introduced into the AR and the

number of moles of oxygen needed for full combustion of the fuel at the given fuel flow rate. Accordingly, when OFR is very close or falls below unity (i.e. OFR < 1), CLG conditions are realized. In this work the experiments carried on at the fuel flow rate of 2 L·min^{-1} are considered as CLG. BMV experiments were carried out at temperatures of 850 and 900 °C. The experimental procedure is given in Table 3. The reactor was cooled down to room temperature in air at the end of each experiment. The composition of the gases arising from the FR was analyzed using an Agilent Micro GC CP-4900 and online gas analyzers (SICK Extractive Gas Analyzer SIDOR).

In reality, the overall air-to-fuel-ratio does not reflect oxygen availability for the fuel in the fuel reactor. The oxygen used for regeneration of the oxygen carrier is limited by the oxygen transferred to fuel in the fuel reactor. The availability of oxygen in the FR is related to bed mass and circulation, which were both held constant during the tests, while fuel flow was varied. To facilitate the comparison for CLG, an effective air ratio is used in the evaluation below.

2.5. Data evaluation

In this work, the effect of temperature and fuel flow rate on syngas fraction, fraction of methane in the flue gas from the FR, and H_2/CO ratio are given based on Effective Air Ratio (λ_{eff}) which is defined as the ratio between the oxygen which is transferred from AR to the gas phase in FR by the oxygen carriers and the oxygen needed for full combustion of the fuel (stoichiometric oxygen).

$$\lambda_{eff} = \frac{oxygen\ transferred\ from\ AR\ to\ FR}{oxygen\ needed\ for\ full\ combustion} \qquad [3]$$

The transferred oxygen from the AR to AR exclusively is the oxygen that reacted with the fuel in the FR. Therefore, the remaining oxygen in

Table 2
The composition of the synthetic biomass volatiles fuel (BMV).

Component	Fraction (vol%)	Carbon fraction (atomic %)	LHV (MJ/ m_n^3)
CO	43	55.1	12.6
H_2	30	–	10.8
CH_4	20	25.6	35.8
C_2H_4	6	15.4	59.0
C_3H_6	1	3.8	85.9
Total	100	99.9	20.2

Table 3
Experimental conditions employed during experimental campaigns.

Fuel	FR fuel flow [L·min^{-1}]	FR temperature [°C]	AR air flow [L·min^{-1}]	Run time [hrs]
Ilmenite				
Syngas	1	900	8	2
BMV	0.6 – 2	850–900	9	12
LD Slag				
Syngas	1	900	8	2
BMV	0.6 – 2	850–900	9	7

the lattice of the oxygen carrier is returned to the AR and is not considered in the definition of the λ_{eff}. In this sense, the Effective Air Ratio is equal to the gas conversion efficiency (η_{gas}) in the FR [38]:

$$\lambda_{eff} = \eta_{gas} = 1 - \Omega_{OD} \qquad [4]$$

where Ω_{OD} is the oxygen demand:

$$\Omega_{OD} = \frac{0.5x_{CO} + 2x_{CH_4} + 0.5x_{H_2} + 3x_{C_2H_4} + 4.5x_{C_3H_6}}{\Phi_0(x_{CO} + x_{CH_4} + 2x_{C_2H_4} + 3x_{C_3H_6})} \qquad [5]$$

Here x_i is the volume fraction of the gas i and Φ_0 is the oxygen to carbon molar ratio of the fuel [n_{O_2} required for combustion/kg fuel]/ [n_C/kg fuel] [39]:

$$\Phi_0 = \frac{0.5y_{CO} + 2y_{CH_4} + 0.5y_{H_2} + 3y_{C_2H_4} + 4.5y_{C_3H_6}}{y_{CO} + y_{CH_4} + 2y_{C_2H_4} + 3y_{C_3H_6}} \qquad [6]$$

where y is the volume fraction of species i in the fuel based on the composition given in Table 2. For the fuel used in this work, Φ_0 is equal to 1.27.

λ_{eff} depends mainly on the fuel flow rate, temperature, and nature of the oxygen carries as the oxygen uptake and reactivity varies for the different materials. Lower fuel flow gives higher gas conversion, thus higher effective air ratio.

The syngas fraction in the product gas (f_{syngas}), as an important measure for CLG, is defined as the fraction of H_2 and CO in the gas leaving the reactor, on a dry basis.

$$f_{syngas} = \frac{x_{CO} + x_{H_2}}{x_{CO} + x_{CO_2} + x_{CH_4} + x_{H_2} + x_{C_2H_4} + x_{C_3H_6}} \qquad [7]$$

The carbon fraction, f_i, is the molar ratio of species i normalized to total carbon and is defined as follows:

$$f_i = \frac{x_i}{x_{CO} + x_{CO_2} + x_{CH_4} + 2x_{C_2H_4} + 3x_{C_3H_6}} \qquad [8]$$

where i is any of CO, CO_2, CH_4, or C_nH_{2n} and $\times$ is the volumetric ratio and the denominator represents the total carbon in the outlet stream. To assess the remaining amount of a given species in the fuel gas, the ratio between the carbon fraction in the outlet and inlet stream is used:

FR conversion ratio = $\varphi_i = \frac{f_i^{out}}{f_i^{in}}$ [9]

For the synthetic BMV used in this work, f_i^{in} of CO, CH_4, and C_2H_4 and C_3H_6 are 0.55, 0.26, 0.08 and 0.01, respectively, given that the total carbon content, i.e. the denominator in eq. 8, is 0.78. In the case of hydrogen, the φ_i is ratio between the molar ratio of hydrogen in the inlet fuel and the products (FR outlet).

As syngas is intended to be the main product in CLG, the syngas to hydrocarbon ratio is introduced as a measure of CLG in terms of delivery of CO and H_2. The syngas to hydrocarbon ratio is defined as follows:

$$\text{syngas to hydrocarbon ratio} = \frac{0.5x_{CO} + 0.5x_{H_2}}{2x_{CH_4} + 3x_{C_2H_4} + 4.5x_{C_3H_6}} \qquad [10]$$

3. Results and discussion

3.1. Activation of the oxygen carriers

The FR was purged with argon before operating with fuel to prevent direct mixing of air and fuel. As an example, the concentrations of the gases from the FR and AR during the activation phase of ilmenite at 900 °C with syngas (1 Lmin^{-1}) are illustrated in Fig. 3. The vertical dashed line shows where syngas started, therefore, CO_2 and CO increased in the FR and oxygen decreased in the AR as a result of uptake of oxygen by the oxygen carriers that are circulating between the AR and FR. The sudden increase in CO_2 at around minute 20 is due to the stopping of argon flow into the FR. Argon flow is kept at the start of the fuel purge to assure mild variations in the FR environment and prevent
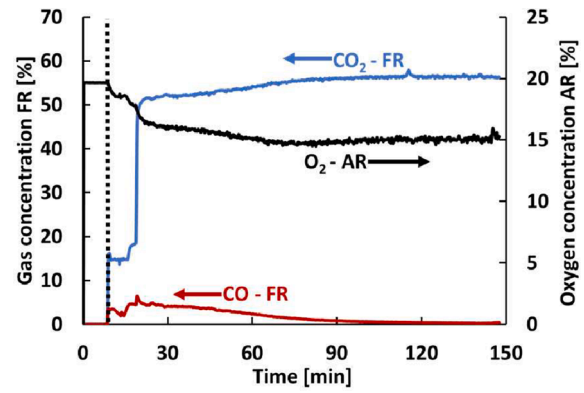

Fig. 3. The concentration of the FR and AR outlet (dry basis) during the activation of ilmenite at 900 °C with syngas. The dashed line shows the start of the fuel addition.

defluidization. Therefore, CO_2 is diluted for a few minutes while argon is still running into the FR.

After almost 20 min from the start of the fuel injection, the concentration of CO_2 increased gradually upon higher conversion of CO. Simultaneously, the oxygen concentration in AR outlet decreased which is due to the increasing capacity of oxygen carrier to transfer oxygen from the AR to FR because of activation. As seen in Fig. 3, the oxygen carriers are activated when CO concentration from FR reached its minimum, <0.5% was detected by the gas analyzer. In other words, CO_2 from the FR and oxygen from the AR become stable, meaning that oxygen transfer from AR to FR has reached the highest possible level at the given conditions. The outlet concentrations from the FR do not sum up to 100% since the loop seals of the 300 W reactor are fluidized by argon that mixes with the FR and AR outlet streams.

3.2. Carbon fraction – the measure of the performance

The carbon fraction (f_i) as calculated from eq.8, in the outlet gas from the FR gives the first assessment of the experiments with ilmenite and LD Slag and how these particles differ in operation. The carbon fraction of CO, CO_2, and CH_4 in the exhaust gas from FR for both particles is shown in Fig. 4 as a function of λ_{eff}. The fuel flow was used to vary λ_{eff}, and high values of λ_{eff} correspond to low fuel flow rates.

The first feature in Fig. 4 is the range of λ_{eff}. At 900 °C, higher λ_{eff} was reached independent of the oxygen carrier used, which can be ascribed to increase the reactivity of the particles with temperature. In the case of ilmenite, higher λ_{eff} was reached that that indicates a higher reactivity of ilmenite as compared to LD Slag. For the ease of comparison, the corresponding values of λ_{eff} at different conditions employed in this work are given in Table 4.

Apart from ilmenite showing a better gas conversion than LD Slag, the conversion ratio, Eq. 9, of hydrogen and CO was somewhat higher for ilmenite for the lower values of λ_{eff} relevant for gasification (see Fig. 5a and b). Thus, ilmenite shows lower conversion of CO and H_2 for similar λ_{eff}, which means a higher conversion of other gases, i.e. hydrocarbons. Consequently, at the same effective air ratio, ilmenite shows higher conversion of methane compared to LD slag, Fig. 5c. There is no notable difference in the conversion ratio of C_2H_4. Also, no C_3H_6 was detected by the GC.

Higher temperature is in favor of conversion of CH_4 and C_2H_4, Fig. 5c and d, which consequently means more syngas. The conversion ratio of CH_4 in the case of LD Slag increased to around 1 at low λ_{eff} meaning that almost no methane is converted at the highest fuel flow rate tested.

3.3. Syngas fraction

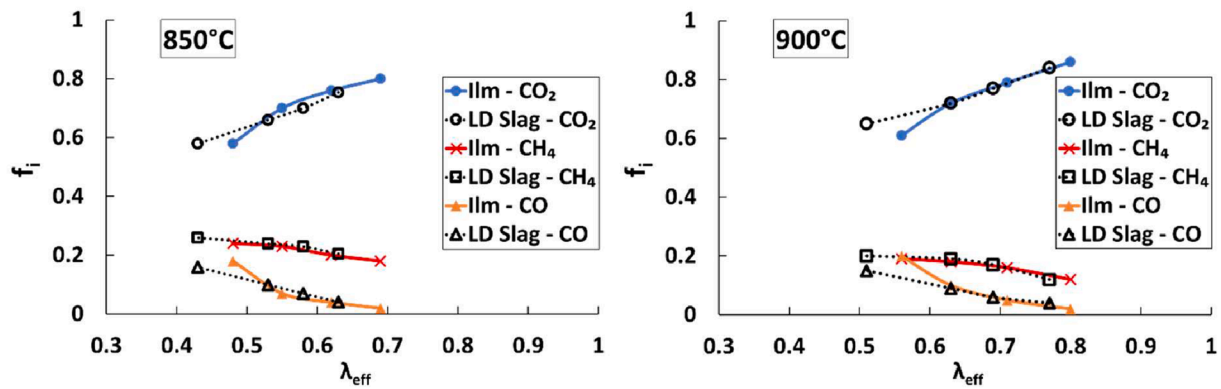The syngas fraction in the outlet of the FR is one of the important

Fig. 4. Carbon fraction of CO, CO_2, and CH_4 in the FR outlet.

Table 4
Effective air ratio (λ_{eff}) corresponding to fuel flow rates and oxygen carriers used in this work.

| BMV flow (Lmin^{-1})	$\lambda_{eff} = \eta_{gas} = 1 - \Omega_{OD}$			
	T = 850°C		T = 900°C	
	Ilm	LD Slag	Ilm	LD Slag
0.6	0.69	0.63	0.80	0.77
0.9	0.62	0.58	0.71	0.69
1.2	0.55	0.53	0.63	0.63
2	0.48	0.43	0.56	0.51

factors in the CLG process. As shown in Fig. 6, both the syngas fraction and the syngas to hydrogen ratios, was higher for ilmenite at the higher fuel flows. Especially at 900 °C and the lowest λ_{eff} there is a notable increase in syngas fraction and syngas to carbon ratio, for ilmenite

which indicates that higher temperatures are in favor of syngas.

3.4. H_2/CO ratio

Another important factor in CLG is the molar ratio of H_2 and CO and H_2/CO ratio around 2 is preferred for probable downstream processes such as Fischer Tropsch synthesis where liquid hydrocarbon can be produced from hydrogen and carbon monoxide [12]. This ratio can be altered downstream by the water–gas-shift reaction, but it would be an advantage if this ratio would be high already in gas coming from the FR. The H_2/CO ratio of ilmenite and LD Slag is given in Fig. 7.

The H_2/CO ratio falls with temperature which is also expected for the endothermic nature of the water–gas-shift reaction. LD Slag showed lower H_2/CO compared to ilmenite, but not for low λ_{eff} which is relevant for CLG. The general trend in Fig. 7 is a decrease in the H_2/CO ratio with fuel flow but the decrease is more pronounced for ilmenite. It should be mentioned that the H_2/CO ratio discussed in this work does not reflect
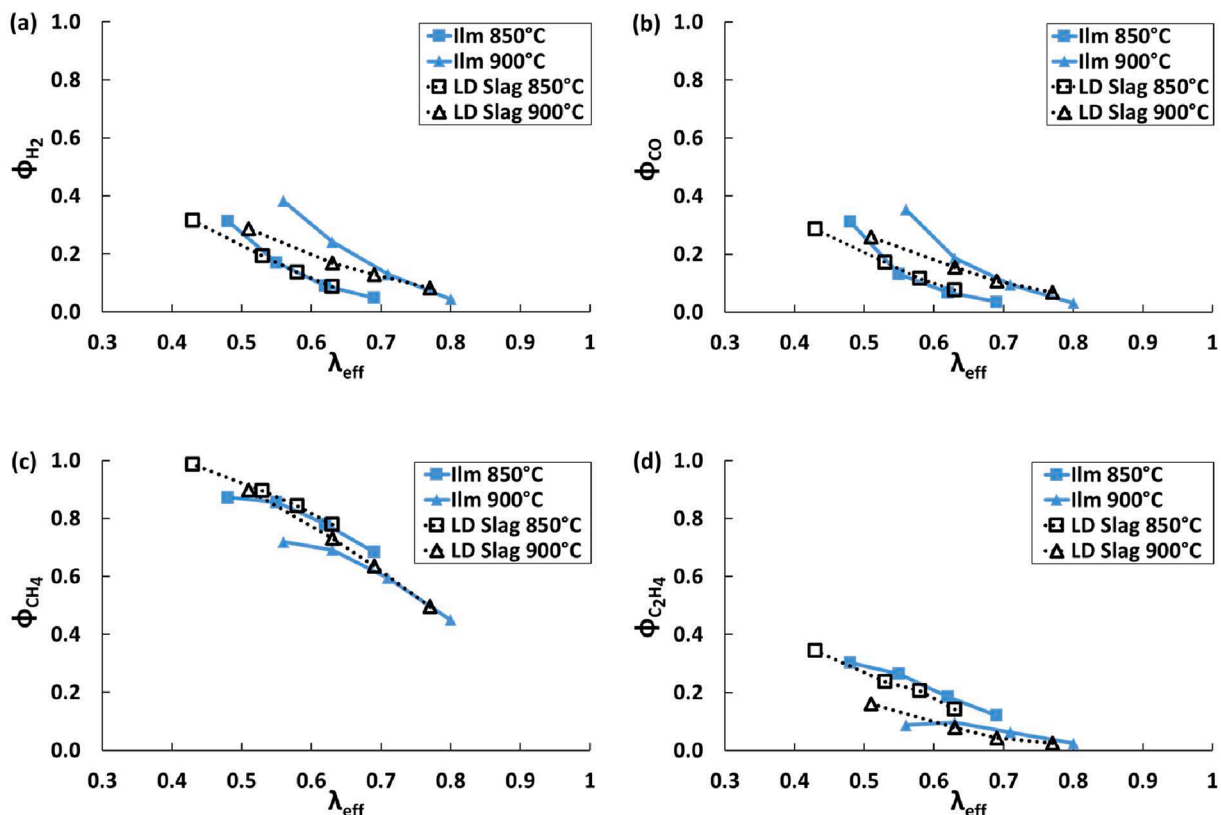
Fig. 5. Conversion ratio of H_2 (a), CO (b), CH_4 (c), and C_2H_4 (d) versus λ_{eff}.
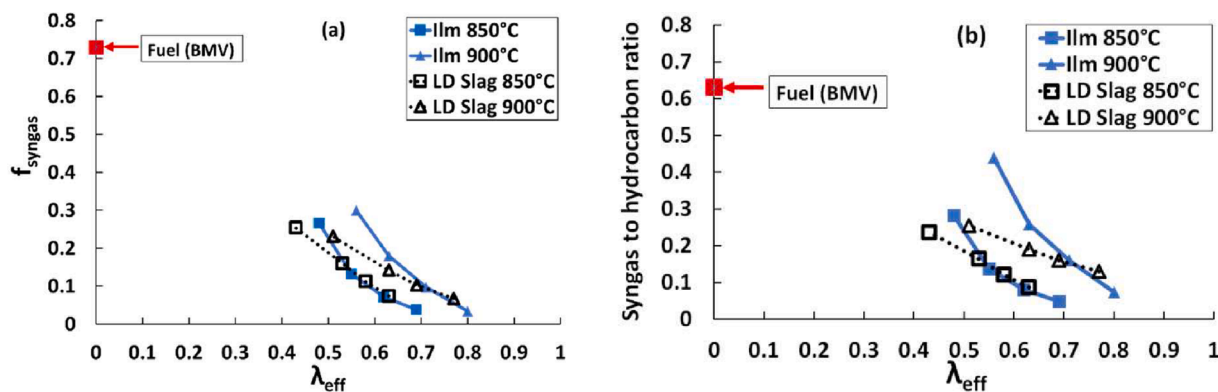
Fig. 6. Syngas fraction (a) and syngas to hydrocarbon ratio (b). The red marks show the corresponding value for the fuel (BMV) used in this work. (For interpretation of the references to colour in this figure legend, the reader is referred to the web version of this article.)
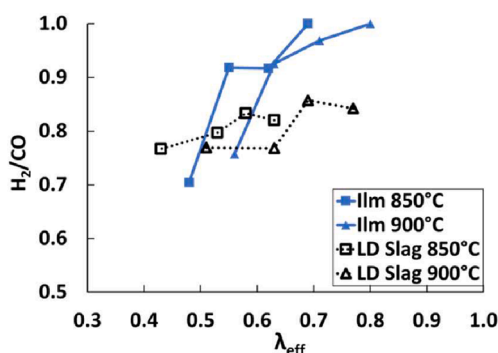

Fig. 7. H_2/CO ratio of EB and SC.

the syngas that can be formed via char gasification when real solid biomass is gasified in a fluidized bed reactor.

3.5. Analysis of the particles

3.5.1. Attrition and particle size distribution (PSD)

The lifetime of the particles is one of the main parameters for the selection of suitable oxygen carriers for the chemical looping process. At chemical looping conditions, particles are exposed to high velocities, especially in the air reactor, hence subject to impact and thermochemical stress. Thus, particles undergo mechanical erosion in a circulating fluidized bed reactor and they turn to dust or fines and may leave the reactor together with the gas flow [39]. It can be expected that the oxygen carriers show a higher propensity for attrition at CLG conditions due to a higher reduction in the fuel reactor. The density of the particles before and after the experiments is an indicator of possible changes in the physical properties of the particles. Density and attrition rates of the fresh and used particles in size range of <212 μm tested in this work are given in Table 5. The density of the particles is the mean of five measurements with a standard deviation of around 0.1.

Moldenhauer et al. [5] used LD Slag in the similar experimental setup to this work and reported attritaion rate of 0.58 w%hr^{-1} after 20 h of

Table 5
Bulk density and attrition rate of the fresh (calcined) and used particles. Total operation corresponds to the time with fluidization and circulation at high temperature with fuel or inert conditions in FR.

Particle	Bulk Density-Fresh (calcined) [gcm^{-3}]	Bulk Density-Used [gcm^{-3}]	Attrition [w %hr^{-1}]	Total operation [hrs]
Ilm	2.0	1.9	0.2	12
LD Slag	1.4	1.2	0.4	7

operation with syngas and methane at 800 – 900 °C at CLC conditions. Moldenhauer et al. [3] also performed CLC experiments with five types of manganese ores using the same fuel and reactor setup used in this work and reported attrition rates varying between 0.05 and 1.12 w%hr^{-1}. It is seen that the attrition rates of both ilmenite and LD Slag observed in this work sit in the middle range of what was reported before in the literature. However, it should be reminded that the particle underwent CLG conditions in this work which are rather harsher than CLC ones.

Both oxygen carriers showed some decrease in density after the operation. However, ilmenite is notably denser than LD Slag with less attrition during operation at high temperatures. As shown in Fig. 8, particle size distribution (PSD) of LD Slag shifted toward smaller particles in agreement with attrition data in Table 5. In the case of ilmenite, the PSD of the used particles showed a peak in the interval 90–120 μm.

3.5.2. Phase composition

X-ray powder diffractometry (XRD) was performed to analyze the crystal structure of different samples of ilmenite and LD slag. The fresh samples after calcination in air at 950 °C for 24 h, used oxidized samples extracted from the air reactor after the experiments, and particles from the FR filter after the operation with fuel as the reduced samples were tested. The main crystalline phases of the particles are given in Table 6.

The active parts of ilmenite are iron and titanium. The XRD of the fresh calcined ilmenite revealed $(Ti,Fe)_2O_3$ and $FeTiO_3$ and some free hematite (Fe_2O_3) as the major components which are in agreement with the literature and showed that ilmenite was in the most oxidized state after calcination [40,41]. In the ilmenite used samples, TiO_2 is present which can be a result of physical segregation of Fe_2TiO_5 during the continuous operation [40]. $(Fe,Ti)_2O_3$ is the reduced form of Fe_2TiO_5 which was possibly formed via the compound $Ti_3Fe_3O_{10}$.

The diffractograms were very complicated in the case of LD Slag, with diverse interpretations possible. The fresh calcined sample contained $(Mg,Fe)O$ and many minor phases composed of oxides of Fe, Ca, Mg, Al, and V. In general, XRD revealed more major phases in the used sample of LD Slag which may mean that the used particles were more homogenized than the fresh calcined ones. Hildor et al. [33] detected CaO in the fully oxidized samples after their experiments, but in this work no sign of this phase was found in the used or fresh samples. Ca $(OH)_2$ was reported by Moldenhauer et al. [5] in the reduced LD Slag samples; however, we could not detect this phase in the reduced samples.

4. Conclusion

Ilmenite and LD Slag were tested in continuous operation in a 0.3 kW reactor. A gas mixture representing biomass volatiles resulting from biomass gasification and pyrolysis was used as fuel. Experiments were carried out at 850 and 900 °C with regard to CLC and CLG. The fraction
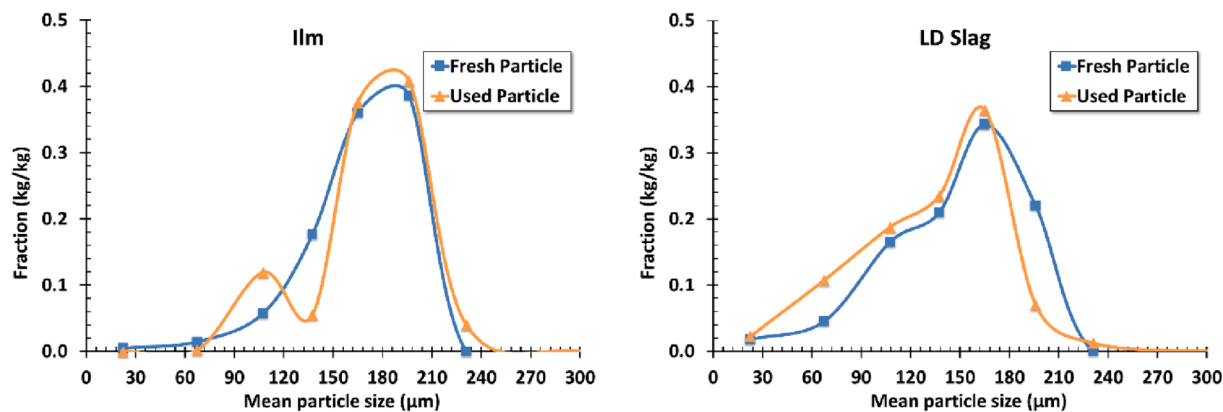
Fig. 8. Particle size distribution (PSD) of fresh and used (fully oxidized) oxygen carriers.

Table 6

Main crystalline phases identified by XRD in fresh, used, and reduced samples used in this work.

	Fresh (calcined)	Used (fully oxidized)	Reduced
Ilm	$(Ti,Fe)_2O_3$, $FeTiO_3$, Fe_2O_3	Fe_2O_3, TiO_2, Fe_2TiO_5, $Ti_3Fe_3O_{10}$	$(Ti,Fe)_3O_4$, $(Fe,Ti)_2O_3$, Fe_3O_4, TiO_2
LD Slag	$(Fe,Mg)O$ $(Mg,Fe,Ca,Si)_xO_y$	$Ca_2Fe_2O_5$, MgO, Ca_2SiO_4, Ca_2SiO_4, $CaMgV_2O_7$	$Ca_2Fe_2O_5$, $(Mg,Mn,Fe)_3O_4$, Ca_3SiO_5

of CO, CO_2, and CH_4, the syngas fraction, the conversion ratio, and H_2/ CO ratio in the outlet of the FR showed that:

   i) gas conversion was generally higher for ilmenite, independent of temperature and fuel flow

   ii) methane conversion was higher in the case of ilmenite both at similar effective air ratio and for similar fuel flow

   iii) syngas fraction and syngas to hydrocarbon ratio, was higher for ilmenite compared to LD Slag at a similar effective air ratio

   iv) the syngas fraction and the syngas to hydrocarbon ratios, were generally higher at a higher temperature for both oxygen carriers

   v) LD Slag showed release of oxygen at inert conditions

It is concluded that for CLC application ilmenite gives better gas conversion. From CLG point of view, ilmenite delivered more syngas – thanks to the higher methane conversion compared to LD Slag. Based on the particle characterization after 12 h of operation with ilmenite and 7 h with LD Slag, it was also found that LD Slag is more prone to attrition. The particle size distribution also revealed that LD Slag shifted to the smaller particle sizes. Although ilmenite appears to be better for both CLC and CLG, from the economic point of view LD Slag may be promising and beneficial as an industrial waste material.

CRediT authorship contribution statement

Ali Hedayati: Data curation, Formal analysis, Methodology, Writing – original draft, Writing – review & editing. **Amir H. Soleimanisalim:** Data curation, Formal analysis. **Tobias Mattisson:** Funding acquisition, Methodology, Project administration, Supervision, Validation, Writing – review & editing. **Anders Lyngfelt:** Investigation, Methodology, Resources, Validation, Writing – review & editing.

Declaration of Competing Interest

The authors declare that they have no known competing financial interests or personal relationships that could have appeared to influence the work reported in this paper.

Acknowledgment

References

[1] IPCC, 2014. Climate Change 2014: Synthesis Report. Contribution of Working Groups I, II and III to the Fifth Assessment Report of the Intergovernmental Panel on Climate Change. Geneva, Switzerland: 2014.

[2] Karami D, Soleimanisalim AH, Sedghkerdar MH, Mahinpey N. Preparation of Novel Oxygen Carriers Supported by Ti, Zr-Shelled γ-Alumina for Chemical Looping Combustion of Methane. Ind Eng Chem Res 2020;59(7):3221–8. https://doi.org/10.1021/acs.iecr.9b06832.

[3] Moldenhauer P, Sundqvist S, Mattisson T, Linderholm C. Chemical-looping combustion of biomass-volatiles with manganese-ore oxygen carriers. Int J Greenh Gas Control 2018;71:239–52. https://doi.org/10.1016/J.IJGGC.2018.02.021.

[4] Mendiara T, García-Labiano F, Abad A, Gayán P, de Diego LF, Izquierdo MT, et al. Negative CO2 emissions through the use of biofuels in chemical looping technology: a review. Appl Energy 2018;232:657–84. https://doi.org/10.1016/j.apenergy.2018.09.201.

[5] Moldenhauer P, Linderholm C, Rydén M, Lyngfelt A. Avoiding CO 2 capture effort and cost for negative CO 2 emissions using industrial waste in chemical-looping combustion/gasification of biomass. Mitig Adapt Strateg Glob Chang 2020;25(1): 1–24. https://doi.org/10.1007/s11027-019-9843-2.

[6] Adánez J, Abad A, Mendiara T, Gayán P, de Diego LF, García-Labiano F. Chemical looping combustion of solid fuels. Prog Energy Combust Sci 2018;65:6–66. https://doi.org/10.1016/J.PECS.2017.07.005.

[7] Lyngfelt A. Chemical-looping combustion of solid fuels – status of development. Appl Energy 2014;113:1869–73. https://doi.org/10.1016/J.APENERGY.2013.05.043.

[8] Lyngfelt A, Leckner B. A 1000 MWth boiler for chemical-looping combustion of solid fuels – discussion of design and costs. Appl Energy 2015;157:475–87. https://doi.org/10.1016/J.APENERGY.2015.04.057.

[9] Samprón I, de Diego LF, García-Labiano F, Izquierdo MT, Abad A, Adánez J. Biomass Chemical Looping Gasification of pine wood using a synthetic Fe2O3/Al2O3 oxygen carrier in a continuous unit. Bioresour Technol 2020;316:123908. https://doi.org/10.1016/j.biortech.2020.123908.

[10] Lin Y, Wang H, Wang Y, Huo R, Huang Z, Liu M, et al. Review of biomass chemical looping gasification in China. Energy Fuels 2020;34(7):7847–62. https://doi.org/10.1021/acs.energyfuels.0c01022.

[11] Nadgouda SG, Guo M, Tong A, Fan LS. High purity syngas and hydrogen coproduction using copper-iron oxygen carriers in chemical looping reforming process. Appl Energy 2019;235:1415–26. https://doi.org/10.1016/j.apenergy.2018.11.051.

[12] van Vuuren MJ, Davis BH. Fischer-Tropsch synthesis: compositional modulation study using an iron catalyst. Stud Surf Sci Catal 2007;163:201–15. https://doi.org/10.1016/S0167-2991(07)80480-0.

[13] Mattison T, Hildor F, Li Ye, Linderholm C. Negative emissions of carbon dioxide through chemical-looping combustion (CLC) and gasification (CLG) using oxygen carriers based on manganese and iron. Mitig Adapt Strateg Glob Chang 2020;25(4): 497–517. https://doi.org/10.1007/s11027-019-09860-x.

[14] Kostyniuk A, Grilc M, Likozar B. Catalytic cracking of biomass-derived hydrocarbon tars or model compounds to form biobased benzene, toluene, and xylene isomer mixtures. Ind Eng Chem Res 2019;58(19):7690–705. https://doi.org/10.1021/acs.iecr.9b01219.

[15] Keller M, Leion H, Mattisson T, Thunman H. Investigation of natural and synthetic bed materials for their utilization in chemical looping reforming for tar elimination in biomass-derived gasification gas. Energy Fuels 2014;28(6):3833–40. https://doi.org/10.1021/ef500369c.

[16] Arjmand M, Leion H, Mattisson T, Lyngfelt A. Investigation of different manganese ores as oxygen carriers in chemical-looping combustion (CLC) for solid fuels. Appl Energy 2014;113:1883–94. https://doi.org/10.1016/J.APENERGY.2013.06.015.

[17] Andersson V, Soleimanisalim AH, Kong X, Hildor F, Leion H, Mattisson T, et al. Alkali-wall interactions in a laboratory-scale reactor for chemical looping combustion studies. Fuel Process Technol 2021;217:106828. https://doi.org/10.1016/j.fuproc.2021.106828.

[18] Gogolev I, Soleimanisalim AH, Linderholm C, Lyngfelt A. Commissioning, performance benchmarking, and investigation of alkali emissions in a 10 kWth solid fuel chemical looping combustion pilot. Fuel 2021;287:119530. https://doi.org/10.1016/j.fuel.2020.119530.

[19] Ohlemüller P, Ströhle J, Epple B. Chemical looping combustion of hard coal and torrefied biomass in a 1 MWth pilot plant. Int J Greenh Gas Control 2017;65:149–59. https://doi.org/10.1016/J.IJGGC.2017.08.013.

[20] Lyngfelt A, Linderholm C. Chemical-looping combustion of solid fuels – status and recent progress. Energy Procedia 2017;114:371–86. https://doi.org/10.1016/J.EGYPRO.2017.03.1179.

[21] Li D, Xu R, Li X, Li Z, Zhu X, Li K. Chemical looping conversion of gaseous and liquid fuels for chemical production: a review. Energy Fuels 2020;34(5):5381–413. https://doi.org/10.1021/acs.energyfuels.0c01006.

[22] Gogolev I, Linderholm C, Gall D, Schmitz M, Mattisson T, Pettersson JBC, et al. Chemical-looping combustion in a 100 kW unit using a mixture of synthetic and natural oxygen carriers – Operational results and fate of biomass fuel alkali. Int J Greenh Gas Control 2019;88:371–82. https://doi.org/10.1016/j.ijggc.2019.06.020.

[23] Condori O, García-Labiano F, de Diego LF, Izquierdo MT, Abad A, Adánez J. Biomass chemical looping gasification for syngas production using ilmenite as oxygen carrier in a 1.5 kWth unit. Chem Eng J 2021;405:126679. https://doi.org/10.1016/j.cej.2020.126679.

[24] Costa TR, Gayán P, Abad A, García-Labiano F, de Diego LF, Melo DMA, et al. Mn-based oxygen carriers prepared by impregnation for Chemical Looping Combustion with diverse fuels. Fuel Process Technol 2018;178:236–50. https://doi.org/10.1016/j.fuproc.2018.05.019.

[25] Salvi BL, Jindal S. Recent developments and challenges ahead in carbon capture and sequestration technologies. SN Appl Sci 2019;1:885. https://doi.org/10.1007/s42452-019-0909-2.

[26] Liu L, Li Z, Wang L, Zhao Z, Li Y, Cai N. MgO-kaolin-supported manganese ores as oxygen carriers for chemical looping combustion looping combustion 2019. doi: 10.1021/acs.iecr.9b05267.

[27] Lyngfelt A, Brink A, Langørgen Ø, Mattisson T, Rydén M, Linderholm C. 11,000 h of chemical-looping combustion operation—where are we and where do we want to go? Int J Greenh Gas Control 2019;88:38–56. https://doi.org/10.1016/j.ijggc.2019.05.023.

[28] Abanades JC, Arias B, Lyngfelt A, Mattisson T, Wiley DE, Li H, et al. Emerging CO2 capture systems. Int J Greenh Gas Control 2015;40:126–66. https://doi.org/10.1016/j.ijggc.2015.04.018.

[29] Hedayati A, Soleimanisalim AH, Linderholm CJ, Mattisson T, Lyngfelt A. Experimental evaluation of manganese ores for chemical looping conversion of synthetic biomass volatiles in a 300 W reactor system. J Environ Chem Eng 2021;9. https://doi.org/10.1016/j.jece.2021.105112.

[30] Xu L, Schwebel GL, Knutsson P, Leion H, Li Z, Cai N. Performance of industrial residues as low cost oxygen carriers. Energy Procedia 2017;114:361–70. https://doi.org/10.1016/j.egypro.2017.03.1178.

[31] Adanez J, Abad A, Garcia-Labiano F, Gayan P, de Diego LF. Progress in chemical-looping combustion and reforming technologies. Prog Energy Combust Sci 2012;38(2):215–82. https://doi.org/10.1016/j.pecs.2011.09.001.

[32] Chand S, Paul B, Kumar M. Sustainable approaches for LD slag waste management in steel industries: a review. Metallurgist 2016;60(1-2):116–28. https://doi.org/10.1007/s11015-016-0261-3.

[33] Hildor F, Mattisson T, Leion H, Linderholm C, Rydén M. Steel converter slag as an oxygen carrier in a 12 MWth CFB boiler – ash interaction and material evolution. Int J Greenh Gas Control 2019;88:321–31. https://doi.org/10.1016/J.IJGGC.2019.06.019.

[34] Hu Q, Shen Ye, Chew JW, Ge T, Wang C-H. Chemical looping gasification of biomass with Fe2O3/CaO as the oxygen carrier for hydrogen-enriched syngas production. Chem Eng J 2020;379:122346. https://doi.org/10.1016/j.cej.2019.122346.

[35] Condori O, García-Labiano F, de Diego LF, Izquierdo MT, Abad A, Adánez J. Biomass chemical looping gasification for syngas production using LD Slag as oxygen carrier in a 1.5 kWth unit. Fuel Process Technol 2021;222:106963. https://doi.org/10.1016/j.fuproc.2021.106963.

[36] Johannsen K. Experimental testing of oxygen carriers in a 300 W chemical-looping combustion reactor. Chalmers University of Technology; 2018.

[37] Larsson A, Israelsson M, Lind F, Seemann M, Thunman H. Using ilmenite to reduce the tar yield in a dual fluidized bed gasification. System 2014;28(4):2632–44. https://doi.org/10.1021/ef500132p.

[38] Linderholm C, Knutsson P, Schmitz M, Markström P, Lyngfelt A. Material balances of carbon, sulfur, nitrogen and ilmenite in a 100kW CLC reactor system. Int J Greenh Gas Control 2014;27:188–202. https://doi.org/10.1016/j.ijggc.2014.05.001.

[39] Linderholm C, Schmitz M, Biermann M, Hanning M, Lyngfelt A. Chemical-looping combustion of solid fuel in a 100 kW unit using sintered manganese ore as oxygen carrier. Int J Greenh Gas Control 2017;65:170–81. https://doi.org/10.1016/j.ijggc.2017.07.017.

[40] Cuadrat A, Abad A, Adánez J, de Diego LF, García-Labiano F, Gayán P. Behavior of ilmenite as oxygen carrier in chemical-looping combustion. Fuel Process Technol 2012;94(1):101–12. https://doi.org/10.1016/j.fuproc.2011.10.020.

[41] Adánez J, Cuadrat A, Abad A, Gayán P, de Diego LF, García-Labiano F. Ilmenite activation during consecutive redox cycles in chemical-looping combustion. Energy Fuels 2010;24(2):1402–13. https://doi.org/10.1021/ef900856d.